Supplementary Material: Unified Meta-Representation and Feedback Calibration for General Disturbance Estimation

This supplementary material provides supplementary details, proofs, and experimental setups referenced in the main paper: **Unified Meta-Representation and Feedback Calibration for General Disturbance Estimation**. It includes meta-learning configurations, theoretical proofs, simulation and real-world experiment parameters, and additional results to support the claims and methodology presented.

I. Details on Meta-Learning Setups

A. Model Architecture

The meta-learner is a fully-connected neural network with 2 hidden layers. The first layer has 32 neurons and the second layer has 3 neurons (the latent space has a dimension of 3), each with a *Tanh* activation function. The input of the model is a time-delay embedded state $\boldsymbol{z} = [\boldsymbol{x}_t, \boldsymbol{x}_{t-1}, \cdots, \boldsymbol{x}_{t-M}]$, where $\boldsymbol{x}_t$ is the current state and $\boldsymbol{x}_{t-1}, \cdots, \boldsymbol{x}_{t-M}$ are the previous states. The full-connected layer serves as the adaptive layer model parameter $\boldsymbol{\theta}$ obtained by the base-learner in meta-learning and tracked by the adaptive law online.

B. Domain Randomization for Representation Learning

The velocity in the earth-fixed frame (see Section.III) is selected to be the state for the time-delay embedding. The output of the model is the force disturbance $\boldsymbol{d} \in \mathbb{R}^3$. Domain randomization is applied on the initial condition of $\boldsymbol{x}$, hyperparameters of polynomial reference trajectories as well as the magnitude and frequency of the generated force disturbances. 10 groups of initial position, velocity, and Euler angles are randomly sampled within a limited range around the referenced state for each trajectory in the batch simulation. 40 polynomial trajectories are generated with randomly sampled positional waypoints in a limited space with random maximum acceleration ranging from $5m/s$ to $10m/s$ and random discrete nodes ranging from 200 to 400. The disturbances $\bar{\boldsymbol{d}}$ are generated using sinusoidal functions with a magnitude range of $0N$ to $3N$ and frequency from $0Hz$ to $0.5Hz$, which can be regarded as non-structural disturbances. Finally, based on the ablation study, we select a 3-step time-delay embedded representation model for its good trade-off in performance and complexity.

C. Meta-Learning Datasets and Training Setups

The meta-learning dataset is constructed by reshaping the batch simulation data into multiple trajectory segments. Each trajectory segment has a length of $N + M + H$, where N is the regression length, M is the time-delay embedding length and H is the prediction horizon. The regression solver in base-learner outputs the model parameter $\boldsymbol{\theta}$ for the next H steps based on the past N sequential data. For current disturbance prediction, H is set to be 1. Such segments form the dataset *meta-learn*, which are then split into *meta-learn* and *meta-test-test* sets with a ratio of 80% and 20%. The mini-batch size is selected to be 200, i.e., 200 trajectory segments are jointly trained in each iteration. The base-learner uses an L2 regularization with a weight of 0.01 to avoid overfitting, the meta-learner is trained with L1 regularization with a weight of 0.001 to create a sparse representation model. For the meta-learning, the meta-learner is trained with 200 iterations with an initial learning rate of 0.01 with dataset *meta-learn*. A further validation is conducted with the dataset *out-of-distribution*, where the magnitude range and frequency of the generated force disturbances are increased to $0N$ to $5N$ and $0Hz$ to $1Hz$ respectively.

II. Proof of Theorem 1

We prove the convergence of the disturbance estimation error $\tilde{\boldsymbol{d}} = \hat{\boldsymbol{d}} - \boldsymbol{d}$ using *Lyapunov* stability analysis. Consider the positive definite *Lyapunov* function candidate:

$$V = \frac{1}{2}\tilde{\boldsymbol{d}}^\top \tilde{\boldsymbol{d}}. \tag{1}$$

This function measures the squared magnitude of the estimation error.

From the feedback-calibration mechanism (Equation 6.) and the disturbance model $\boldsymbol{d} = \boldsymbol{d}_{model} + \boldsymbol{\gamma}$, we obtain the error dynamics:

$$\dot{\tilde{\boldsymbol{d}}} = \dot{\hat{\boldsymbol{d}}} - \dot{\boldsymbol{d}} = \dot{\boldsymbol{\gamma}} - \boldsymbol{L}\tilde{\boldsymbol{d}} \tag{2}$$

where $\boldsymbol{\gamma}$ is the learning residual satisfying $\|\boldsymbol{\gamma}\| \leq \bar{\gamma}$ by Assumption 1.

Differentiating the *Lyapunov* function yields:

$$\begin{aligned} \dot{V} &= \tilde{\boldsymbol{d}}^\top \dot{\tilde{\boldsymbol{d}}} \\ &= \tilde{\boldsymbol{d}}^\top (\boldsymbol{\gamma} - \boldsymbol{L}\tilde{\boldsymbol{d}}) \\ &= -\tilde{\boldsymbol{d}}^\top \boldsymbol{L}\tilde{\boldsymbol{d}} + \tilde{\boldsymbol{d}}^\top \dot{\boldsymbol{\gamma}} \end{aligned} \tag{3}$$

Applying Young's inequality to the cross term:

$$\tilde{\boldsymbol{d}}^\top \dot{\boldsymbol{\gamma}} \leq \frac{\lambda_m(\boldsymbol{L})}{2} \|\tilde{\boldsymbol{d}}\|^2 + \frac{1}{2\lambda_m(\boldsymbol{L})} \bar{\gamma}^2 \tag{4}$$

where $\lambda_m(\boldsymbol{L})$ is the minimum eigenvalue of $\boldsymbol{L}$. This leads to:

$$\dot{V} \leq -\frac{\lambda_m(\boldsymbol{L})}{2} \|\tilde{\boldsymbol{d}}\|^2 + \frac{1}{2\lambda_m(\boldsymbol{L})} \bar{\gamma}^2 \tag{5}$$

Using the comparison lemma, we obtain the solution:

$$V(t) \leq e^{-\lambda_m(\boldsymbol{L})t} V(0) + \frac{\bar{\gamma}^2}{2\lambda_m(\boldsymbol{L})^2} (1 - e^{-\lambda_m(\boldsymbol{L})t}) \tag{6}$$

The disturbance estimation error converges exponentially to the bounded set:

$$\lim_{t \to \infty} \|\tilde{\boldsymbol{d}}\| \leq \frac{\bar{\gamma}}{\lambda_m(\boldsymbol{L})} \tag{7}$$

This shows that the estimation error remains bounded and can be made arbitrarily small by increasing the feedback gain $\boldsymbol{L}$. The convergence rate is determined by $\lambda_m(\boldsymbol{L})$, with larger gains leading to faster convergence.

A. Proof of Theorem 2

We utilize *Lyapunov* stability analysis to prove the simultaneous convergence of both the disturbance estimation error $\tilde{\boldsymbol{d}}$ and parameter estimation error $\tilde{\boldsymbol{\theta}}$.

Consider the *Lyapunov* function:

$$V = \frac{1}{2} \tilde{\boldsymbol{d}}^\top \tilde{\boldsymbol{d}} + \frac{1}{2} \tilde{\boldsymbol{\theta}}^\top \tilde{\boldsymbol{\theta}}. \tag{8}$$

The online learning residual $\boldsymbol{\zeta}$ is defined as: $\boldsymbol{\zeta} = \boldsymbol{\gamma} + \boldsymbol{\phi}_t(\boldsymbol{z})\tilde{\boldsymbol{\theta}}$, where the learning residual $\boldsymbol{\gamma} = \boldsymbol{d} - \boldsymbol{\phi}_t(\boldsymbol{z})\boldsymbol{\theta}^*$ is augmented with online parameter estimation error $\boldsymbol{\phi}_t(\boldsymbol{z})\tilde{\boldsymbol{\theta}}$.

For simplicity, we assume the concurrent number $N_c = 1$, which refers to a standard composite adaptive law. The proof is similar for $N_c > 1$, but the persistence of excitation condition of $\boldsymbol{\phi}_t(\boldsymbol{z})$ is replaced by a finite time excitation condition [1], [2].

Differentiating V yields:

$$\begin{aligned} \dot{V} &= \tilde{\boldsymbol{d}}^\top \dot{\tilde{\boldsymbol{d}}} + \tilde{\boldsymbol{\theta}}^\top \dot{\tilde{\boldsymbol{\theta}}} \\ &= \tilde{\boldsymbol{d}}^\top (-\boldsymbol{L}\tilde{\boldsymbol{d}} + \dot{\boldsymbol{\zeta}}) + \tilde{\boldsymbol{\theta}}^\top \left(\dot{\boldsymbol{\theta}}^* - \boldsymbol{\phi}_t(\boldsymbol{z})^\top \boldsymbol{P} \left(\boldsymbol{d} - \boldsymbol{\phi}_t(\boldsymbol{z}) \hat{\boldsymbol{\theta}} \right) \right) \\ &= -\tilde{\boldsymbol{d}}^\top \boldsymbol{L}\tilde{\boldsymbol{d}} + \tilde{\boldsymbol{d}}^\top \dot{\boldsymbol{\zeta}} + \tilde{\boldsymbol{\theta}}^\top \dot{\boldsymbol{\theta}}^* - \tilde{\boldsymbol{\theta}}^\top \boldsymbol{P} \boldsymbol{\phi}_t(\boldsymbol{z})^\top \boldsymbol{\phi}_t(\boldsymbol{z}) \tilde{\boldsymbol{\theta}} - \tilde{\boldsymbol{\theta}}^\top \boldsymbol{P} \boldsymbol{\phi}_t(\boldsymbol{z})^\top \boldsymbol{\gamma} \end{aligned} \tag{9}$$

where

$$\begin{aligned}\tilde{\boldsymbol{d}}^\top \dot{\boldsymbol{\zeta}} &= \tilde{\boldsymbol{d}}^\top \dot{\boldsymbol{d}} - \tilde{\boldsymbol{d}}^\top \dot{\boldsymbol{d}}_{model} + \tilde{\boldsymbol{d}}^\top \dot{\boldsymbol{\gamma}} \\ &= \tilde{\boldsymbol{d}}^\top \boldsymbol{\phi}_t(\boldsymbol{z})\dot{\tilde{\boldsymbol{\theta}}} + \tilde{\boldsymbol{d}}^\top \dot{\boldsymbol{\phi}}_t(\boldsymbol{z})\tilde{\boldsymbol{\theta}} + \tilde{\boldsymbol{d}}^\top \dot{\boldsymbol{\gamma}} \\ &= \tilde{\boldsymbol{d}}^\top \boldsymbol{\phi}_t(\boldsymbol{z})\dot{\boldsymbol{\theta}}^* - \tilde{\boldsymbol{d}}^\top \boldsymbol{\phi}_t(\boldsymbol{z})\boldsymbol{P}\boldsymbol{\phi}_t(\boldsymbol{z})^\top(\boldsymbol{\phi}_t(\boldsymbol{z})\tilde{\boldsymbol{\theta}} + \boldsymbol{\gamma}) + \tilde{\boldsymbol{d}}^\top \dot{\boldsymbol{\phi}}_t(\boldsymbol{z})\tilde{\boldsymbol{\theta}} + \tilde{\boldsymbol{d}}^\top \dot{\boldsymbol{\gamma}}.\end{aligned} \tag{10}$$

Applying Young's inequality to the cross terms:

$$\begin{aligned}&\tilde{\boldsymbol{\theta}}^\top \dot{\boldsymbol{\theta}}^* \leq \frac{1}{2}|\lambda_m(\boldsymbol{P}\boldsymbol{\phi}_t(\boldsymbol{z})^\top \boldsymbol{\phi}_t(\boldsymbol{z}))|\tilde{\boldsymbol{\theta}}^\top \tilde{\boldsymbol{\theta}} + \frac{1}{2|\lambda_m(\boldsymbol{P}\boldsymbol{\phi}_t(\boldsymbol{z})^\top \boldsymbol{\phi}_t(\boldsymbol{z}))|}\bar{d_\theta} \\ &- \tilde{\boldsymbol{\theta}}^\top \boldsymbol{P}\boldsymbol{\phi}_t(\boldsymbol{z})^\top \boldsymbol{\gamma} \leq \frac{1}{2}\tilde{\boldsymbol{\theta}}^\top \tilde{\boldsymbol{\theta}} + \frac{1}{2}|\lambda_M(\boldsymbol{P}\boldsymbol{\phi}_t(\boldsymbol{z})^\top)|\bar{\gamma}^2, \\ &\tilde{\boldsymbol{d}}^\top \boldsymbol{\phi}_t(\boldsymbol{z})\dot{\boldsymbol{\theta}}^* \leq \frac{1}{2}\tilde{\boldsymbol{d}}^\top \tilde{\boldsymbol{d}} + \frac{1}{2}|\lambda_M(\boldsymbol{\phi}_t(\boldsymbol{z}))|\bar{d_\theta}^2, \\ &- \tilde{\boldsymbol{d}}^\top \boldsymbol{\phi}_t(\boldsymbol{z})\boldsymbol{P}\boldsymbol{\phi}_t(\boldsymbol{z})^\top \boldsymbol{\phi}_t(\boldsymbol{z})\tilde{\boldsymbol{\theta}} \leq \frac{1}{2}\tilde{\boldsymbol{d}}^\top \tilde{\boldsymbol{d}} + \frac{1}{2}|\lambda_M(\boldsymbol{\phi}_t(\boldsymbol{z})\boldsymbol{P}\boldsymbol{\phi}_t(\boldsymbol{z})^\top \boldsymbol{\phi}_t(\boldsymbol{z}))|\tilde{\boldsymbol{\theta}}^\top \tilde{\boldsymbol{\theta}}, \\ &- \tilde{\boldsymbol{d}}^\top \boldsymbol{\phi}_t(\boldsymbol{z})\boldsymbol{P}\boldsymbol{\phi}_t(\boldsymbol{z})^\top \boldsymbol{\gamma} \leq \frac{1}{2}\tilde{\boldsymbol{d}}^\top \tilde{\boldsymbol{d}} + \frac{1}{2}|\lambda_M(\boldsymbol{\phi}_t(\boldsymbol{z})\boldsymbol{P}\boldsymbol{\phi}_t(\boldsymbol{z})^\top)|\bar{\gamma}^2, \\ &\tilde{\boldsymbol{d}}^\top \dot{\boldsymbol{\phi}}_t(\boldsymbol{z})\tilde{\boldsymbol{\theta}} \leq \frac{1}{2}\tilde{\boldsymbol{d}}^\top \tilde{\boldsymbol{d}} + \frac{1}{2}|\lambda_M(\dot{\boldsymbol{\phi}}_t(\boldsymbol{z}))|\tilde{\boldsymbol{\theta}}^\top \tilde{\boldsymbol{\theta}}, \\ &\tilde{\boldsymbol{d}}^\top \dot{\boldsymbol{\gamma}} \leq \frac{1}{2}|\lambda_m(\boldsymbol{L})|\tilde{\boldsymbol{d}}^\top \tilde{\boldsymbol{d}} + \frac{1}{2|\lambda_m(\boldsymbol{L})|}\bar{d_\gamma}^2,\end{aligned} \tag{11}$$

where $\lambda_m(\boldsymbol{L})$ and $\lambda_M(\boldsymbol{L})$ are the minimum and maximum eigenvalue of $\boldsymbol{L}$, respectively.

Rearranging the terms, we have:

$$\dot{V} \leq -\frac{1}{2}\mu_1 \tilde{\boldsymbol{\theta}}^\top \tilde{\boldsymbol{\theta}} - \frac{1}{2}\mu_2 \tilde{\boldsymbol{d}}^\top \tilde{\boldsymbol{d}} + \delta \tag{12}$$

where:

$$\begin{aligned}\mu_1 &= |\lambda_m(\boldsymbol{P}\boldsymbol{\phi}_t(\boldsymbol{z})^\top \boldsymbol{\phi}_t(\boldsymbol{z}))| - |\lambda_M(\dot{\boldsymbol{\phi}}_t(\boldsymbol{z}))| - |\lambda_M(\boldsymbol{\phi}_t(\boldsymbol{z})\boldsymbol{P}\boldsymbol{\phi}_t(\boldsymbol{z})^\top \boldsymbol{\phi}_t(\boldsymbol{z}))| - 1 \\ \mu_2 &= \lambda_m(\boldsymbol{L})/2 - 2 \\ \delta &= \frac{1}{2}\left(\frac{1}{|\lambda_m(\boldsymbol{P}\boldsymbol{\phi}_t(\boldsymbol{z})^\top \boldsymbol{\phi}_t(\boldsymbol{z}))|} + |\lambda_M(\boldsymbol{\phi}_t(\boldsymbol{z}))|\right)\bar{d_\theta}^2 \\ &\quad + \frac{1}{2}\left(|\lambda_M(\boldsymbol{P}\boldsymbol{\phi}_t(\boldsymbol{z})^\top)| + |\lambda_M(\boldsymbol{\phi}_t(\boldsymbol{z})\boldsymbol{P}\boldsymbol{\phi}_t(\boldsymbol{z})^\top)|\right)\bar{\gamma}^2 \\ &\quad + \frac{1}{2|\lambda_m(\boldsymbol{L})|}\bar{d_\gamma}^2\end{aligned} \tag{13}$$

We can choose the feedback gain $\boldsymbol{L}$ and the adaptive gain $\boldsymbol{P}$ such that: $\mu_1 > 0$ and $\mu_2 > 0$. Based on Assumption 2, δ can be bounded by $\bar{\delta}$. With $\mu = \max(\mu_1, \mu_2)$, we yield:

$$\dot{V} \leq -\frac{\mu}{2}\left(\tilde{\boldsymbol{\theta}}^\top \tilde{\boldsymbol{\theta}} + \tilde{\boldsymbol{d}}^\top \tilde{\boldsymbol{d}}\right) + \bar{\delta} = -\frac{\mu}{2}V + \bar{\delta} \tag{14}$$

We obtain the solution of the above differential inequality:

$$V(t) \leq e^{-\frac{\mu}{2}t}V(0) + \bar{\delta}(1 - e^{-\frac{\mu}{2}t}) \tag{15}$$

Taking the limit as $t \to \infty$, we have:

$$\lim_{t\to\infty} V(t) \leq \bar{\delta} \tag{16}$$

This implies that both $\tilde{\boldsymbol{d}}$ and $\tilde{\boldsymbol{\theta}}$ converge to bounded sets, the bound $\bar{\delta}$ can be further regularized by the design of $\boldsymbol{L}$, $\boldsymbol{P}$ and $\boldsymbol{\phi}_t(\boldsymbol{z})$, which completes the proof.

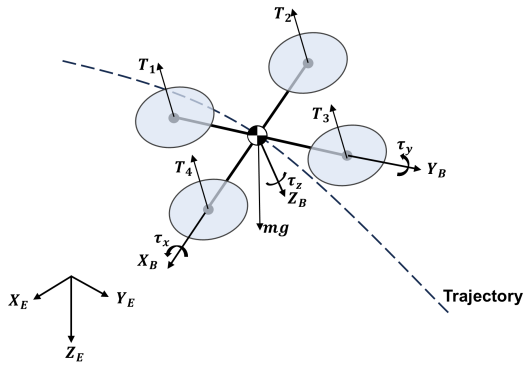

$$
\begin{aligned}
\dot{\boldsymbol{p}} &= \boldsymbol{v} \\
\dot{\boldsymbol{v}} &= -\boldsymbol{Z}_B T/m + g\boldsymbol{Z}_E \\
\dot{\boldsymbol{\Theta}} &= \boldsymbol{W}(\boldsymbol{\Theta})\boldsymbol{\omega} \\
\boldsymbol{J}\dot{\boldsymbol{\omega}} &= -\boldsymbol{\omega} \times (\boldsymbol{J}\boldsymbol{\omega}) + \boldsymbol{\tau} \\
[T, \boldsymbol{\tau}]^\top &= \boldsymbol{C}[T_1, T_2, T_3, T_4]^\top
\end{aligned} \tag{17}
$$

Fig. A1. Quadrotor dynamics.

III. Details in Simulated Experiments

A. Quadrotor Dynamics

The quadrotor system is modeled using a 12-dimensional state vector $\boldsymbol{x} = [\boldsymbol{p}, \boldsymbol{v}, \boldsymbol{\Theta}, \boldsymbol{\omega}]^\top \in \mathbb{R}^{12}$, where $\boldsymbol{p}$ and $\boldsymbol{v}$ represent position and velocity in the earth-fixed frame $\mathcal{E} = \{\boldsymbol{X}_E, \boldsymbol{Y}_E, \boldsymbol{Z}_E\}$, while $\boldsymbol{\omega}$ denotes angular velocity in the body-fixed frame $\mathcal{B} = \{\boldsymbol{X}_B, \boldsymbol{Y}_B, \boldsymbol{Z}_B\}$. The system is controlled through four motor thrust inputs $\boldsymbol{u} = [T_1, T_2, T_3, T_4]^\top \in \mathbb{R}^4$. The transformation between frames is determined by Euler angles $\boldsymbol{\Theta} \in \mathbb{R}^3$. The complete dynamics is described in Figure.A1, where m is the quadrotor mass, g is gravitational acceleration, $\boldsymbol{W}(\cdot)$ is the Euler angle rotation matrix, and $\boldsymbol{C}$ is the control allocation matrix.

B. Tracking Controller

For trajectory tracking, we utilize a differential flatness-based controller (DFBC) [3], [4] as a baseline controller. DFBC consists of an up-level translational controller and a low-level attitude controller, where the former controller outputs a desired acceleration indicating the desired attitude, the input of the low-level controller. The estimated disturbance is removed from the desired acceleration for compensation. The translational controller is designed to minimize the tracking error of the position and velocity with a proportional-integration-derivative (PID) controller:

$$
\boldsymbol{a}_{des} = \boldsymbol{K}_d(\boldsymbol{K}_p(\boldsymbol{p}_d - \boldsymbol{p}) + \boldsymbol{v}_d - \boldsymbol{v}) - \hat{\boldsymbol{d}} + \boldsymbol{a}_d + mg\boldsymbol{Z}_E \tag{18}
$$

where $\hat{\boldsymbol{d}}$ is the estimated force disturbance, $\boldsymbol{p}_d$, $\boldsymbol{v}_d$ and $\boldsymbol{a}_d$ are the desired position, velocity and acceleration computed by the reference trajectory generator, $\boldsymbol{K}_p$, $\boldsymbol{K}_d$ and $\boldsymbol{K}_i$ are the proportional, derivative and integral gains. The low-level attitude controller generates desired thrust and attitude commands based on reference trajectories, which are then converted to motor thrust commands, details refer to [3], [5].

The parameters of the adaptive law and meta-dynamics in simulation are shown in Table.A1.

TABLE A1
Online Adaptation Parameters in Simulation

Parameter	Value	Description
$\boldsymbol{L}$	$\text{diag}\{2.0, 2.0, 2.0\}$	Feedback gain for calibration
$\boldsymbol{P}_{\mathcal{L}_1}$	$2.0 * \boldsymbol{I}_{3\times3}$	Adaptive gain in $\mathcal{L}_1$ adaptive estimator
$f_{\mathcal{L}_1}$	0.25	Low-pass filter gain in $\mathcal{L}_1$ adaptive estimator
$\boldsymbol{P}$	$5.0 * \boldsymbol{I}_{9\times9}$	Adaptive gain for online parameter estimation
$\boldsymbol{\Gamma}$	$5.0 * \boldsymbol{I}_{9\times9}$	Adaptive gain for online parameter estimation
N_c	10	Number of concurrent learning samples
M	3	Time-delay embedding dimension
N	10	Model Regression length

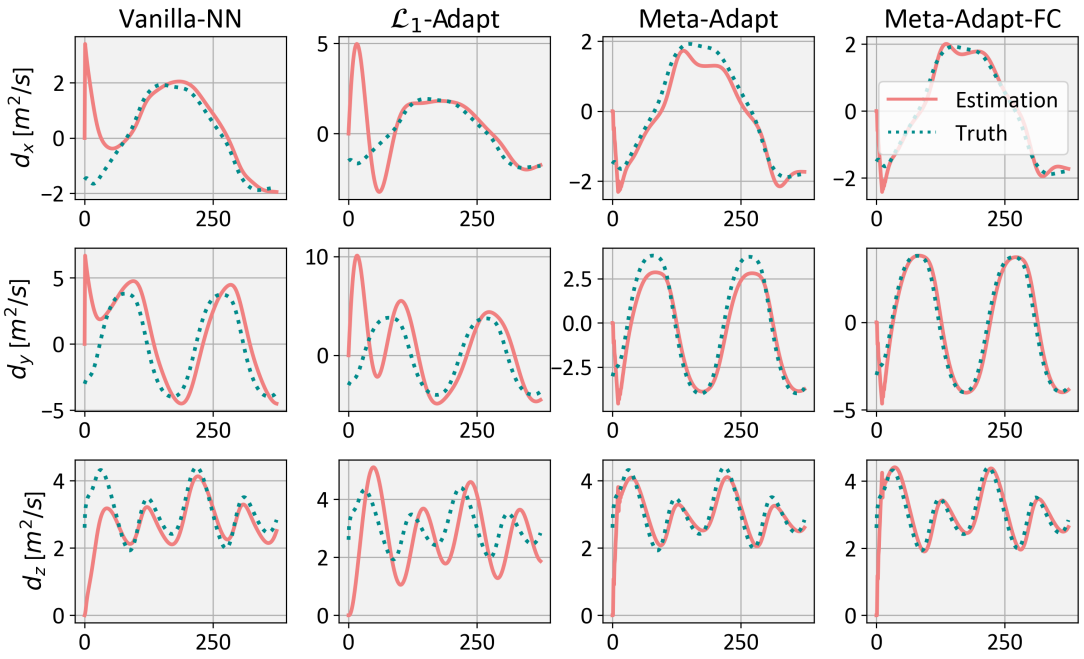

Fig. A2. The results of disturbance estimation in simulated cases.

C. Simulation Environment

The environment in the current simulation is defined as follows: **1.**An external payload of $200g$ on to the quadrotor. **2.**A classical model [6]: $\boldsymbol{RDR}^{\top}\boldsymbol{v}$ is used for drag simulation, where $\boldsymbol{R}$ refers to the current rotational matrix that maps the body-fixed frame $\boldsymbol{\mathcal{B}}$ to the earth-fixed frame $\boldsymbol{\mathcal{E}}$, and $\boldsymbol{D} = \text{diag}\{[0.6, 0.6, 0.1]\}$ is a coefficient matrix. **3.**Constant force disturbance of $1.0N$ is injected into the x and y-axis in $\boldsymbol{\mathcal{B}}$.

D. Results of Disturbance Estimation

4 results out of 7 are chosen to be plotted, where the proposed meta-dynamics (Meta-Adapt) outperforms the previous 2 methods and further improved by the feedback calibration.

IV. Details in Real-World Experiments: Contact Force Estimation

In this section, we provide the details of the contact force estimation. The quadrotor undergoes a series of contact forces provided manually. The IMU measurement of acceleration is collected from the quadrotor, which is then processed by an offline Gaussian Filter. Simulation setups in Section III are used for the contact force estimation. In the simulated environment, the quadrotor is commanded to hover at a fixed position and the contact force is injected into the quadrotor in the earth-fixed frame. The results of the estimation and the boxplots of the contact force estimation are provided in Figure.A3 and Figure.**??**, respectively. Our approach shows the least lagging in disturbance estimation even if the disturbances are completely state-independent and non-structural.

V. Details in Real-World Experiments: Scenario.1 and Scenario.2

A. Tracking Controller

As same as that of the simulated experiments, the tracking controller in real-world experiments is a differential flatness-based controller (DFBC). In the positional controller, an integration controller is added to improve the tracking performance.

$$\boldsymbol{a}_{des} = \boldsymbol{K}_d(\boldsymbol{K}_p(\boldsymbol{p}_d - \boldsymbol{p}) + \boldsymbol{v}_d - \boldsymbol{v}) - \hat{\boldsymbol{d}} + \boldsymbol{a}_d + mg\boldsymbol{Z}_E + \boldsymbol{K}_i \int_0^t (\boldsymbol{p}_d - \boldsymbol{p})dt \tag{19}$$

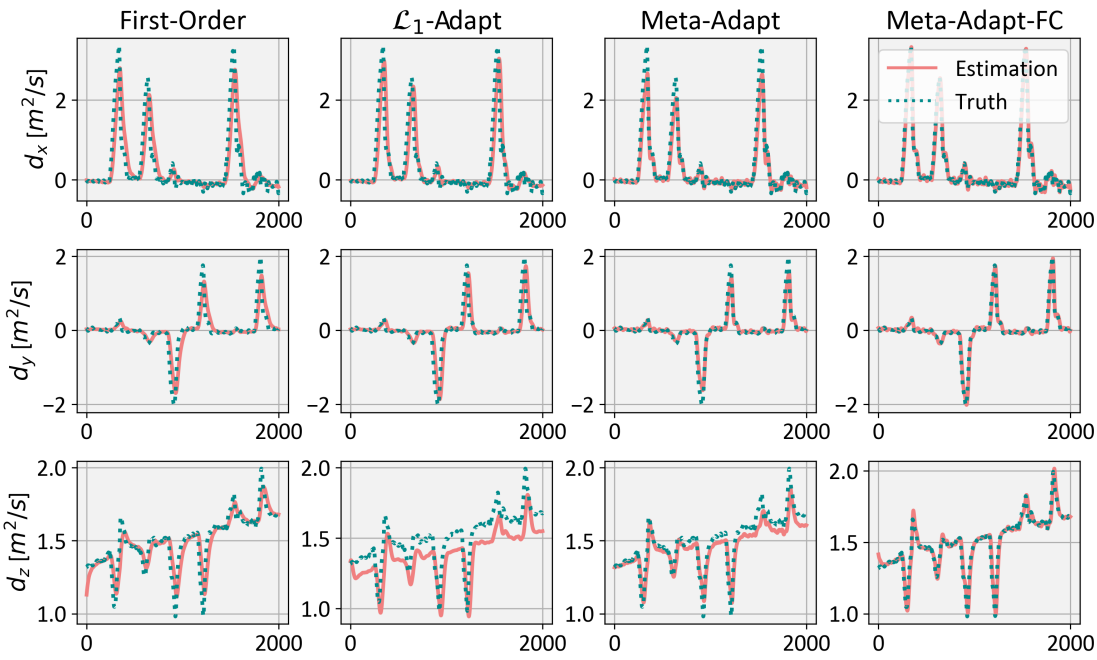

Fig. A3. The results of real-world contact force estimation in simulated cases.

where $\boldsymbol{K}_i$ is the integration gain. The parameters of the adaptive law and meta-dynamics are listed in Table.A2, S1 for Scenario.1 and S2 for Scenario.2:

TABLE A2
ONLINE ADAPTATION PARAMETERS IN REAL-WORLD EXPERIMENTS

Parameter	Value	Description
$\boldsymbol{L}$	$\mathrm{diag}\{0.8, 0.8, 0.8\}$	Feedback gain for calibration
$\boldsymbol{P}$	$4.0 \times \boldsymbol{I}_{9\times9}$	Adaptive gain for parameter estimation
$\boldsymbol{\Gamma}$	$4.0 \times \boldsymbol{I}_{9\times9}$ (control) / $\boldsymbol{0}_{9\times9}$ (estimation)	Adaptive gain for parameter estimation
N	10 and 20 (S1) / 10 (S2)	Model Regression length
N_c	1 (S1) / 5 (S2)	Number of concurrent learning samples
M	0 (S1) / 3 (S2)	Time-delay embedding dimension

B. Results of Disturbance Estimation

The results of disturbance estimation in Scenario.1 and Scenario.2 are shown in Figure.A4 and Figure.A5, respectively. 4 results out of 7 are chosen to be plotted in each scenario, the proposed method outperforms the baseline methods in both scenarios.

C. Ablation Study on the Adaptation Gain

In Scenario.2, the effect of the adaptation gain $\boldsymbol{P}$ is studied. The adaptation gain $\boldsymbol{P}$ is set from $0.1 \times \boldsymbol{I}_{9\times9}$ to $5.0 \times \boldsymbol{I}_{9\times9}$, and the feedback gain $\boldsymbol{L}$ is set to be $0.8 \times \boldsymbol{I}_{3\times3}$. The results are shown in Figure.A6, a higher adaptation gain $\boldsymbol{P}$ leads to faster convergence of the disturbance estimation.

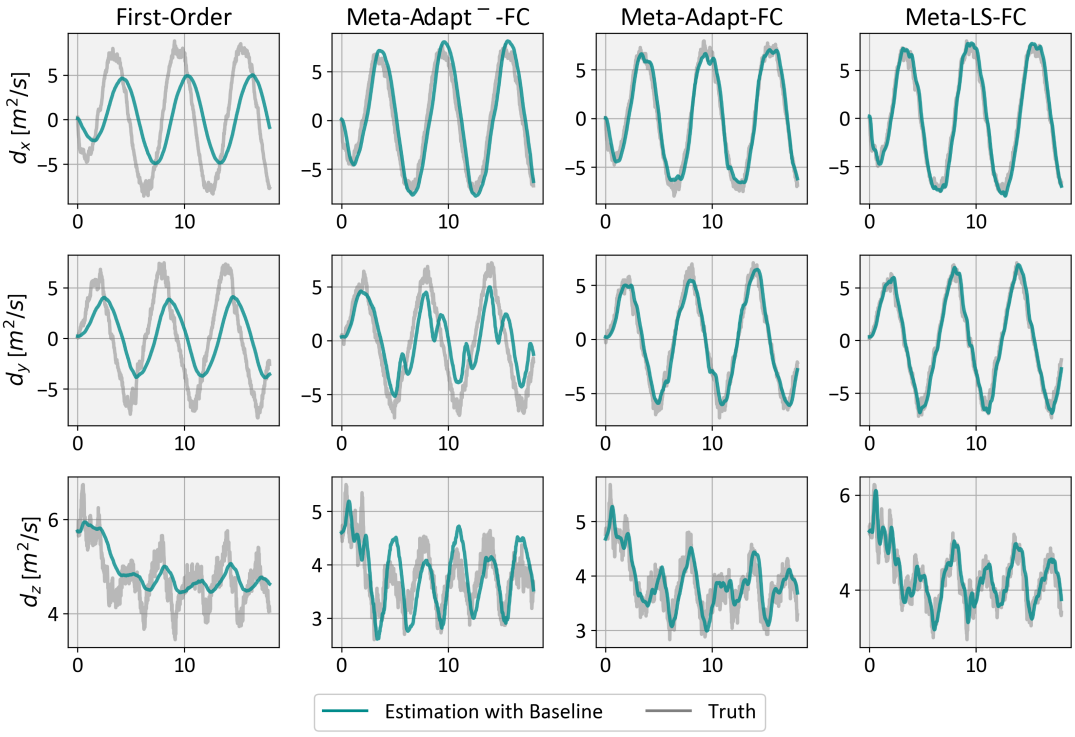

Fig. A4. The results of disturbance estimation in Scenario.1.

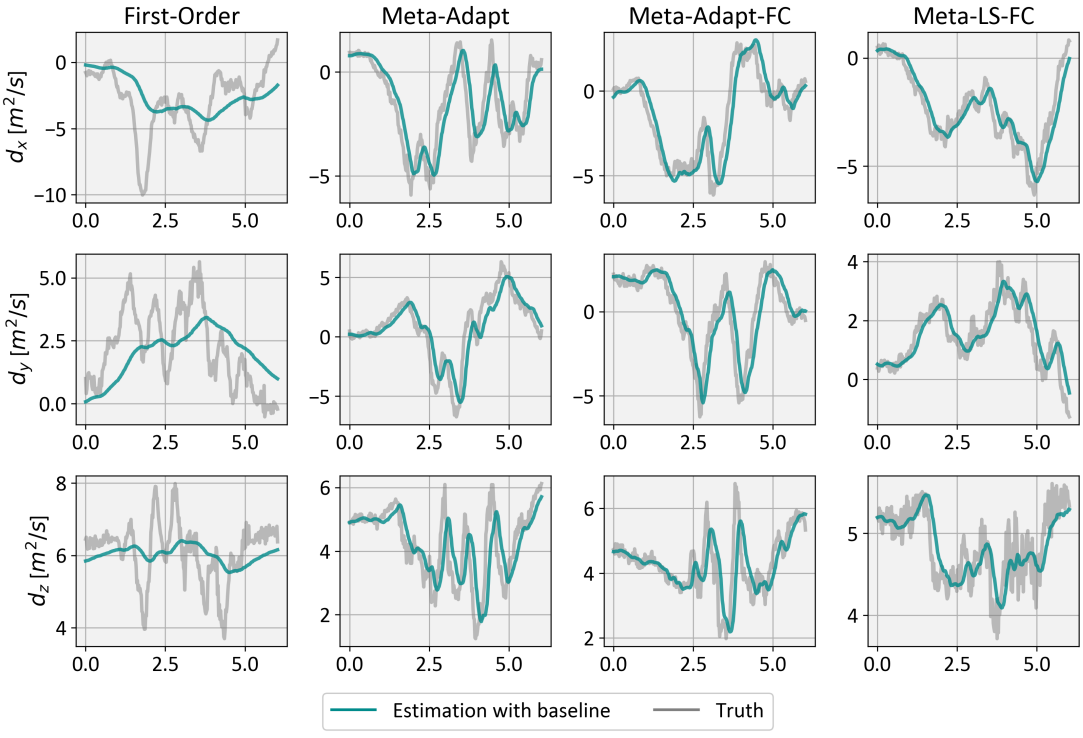

Fig. A5. The results of disturbance estimation in Scenario.2.

REFERENCES

[1] J.-J. E. Slotine, W. Li *et al.*, *Applied nonlinear control*. Prentice hall Englewood Cliffs, NJ, 1991, vol. 199.

[2] G. Chowdhary and E. Johnson, "Concurrent learning for convergence in adaptive control without persistency of excitation," in *49th IEEE Conference on Decision and Control (CDC)*, 2010, pp. 3674–3679.

[3] D. Mellinger and V. Kumar, "Minimum snap trajectory generation and control for quadrotors," in *2011 IEEE International Conference on Robotics and Automation (ICRA)*, 2011, pp. 2520–2525.

[4] B. Morrell, M. Rigter, G. Merewether, R. Reid, R. Thakker, T. Tzanetos, V. Rajur, and G. Chamitoff, "Differential flatness transformations for aggressive quadrotor flight," in *2018 IEEE International Conference on Robotics and Automation (ICRA)*, 2018, pp. 5204–5210.

[5] J. Jia, K. Guo, X. Yu, W. Zhao, and L. Guo, "Accurate high-maneuvering trajectory tracking for quadrotors: A drag utilization method," *IEEE Robotics and Automation Letters*, vol. 7, no. 3, pp. 6966–6973, 2022.

[6] M. Faessler, A. Franchi, and D. Scaramuzza, "Differential flatness of quadrotor dynamics subject to rotor drag for accurate tracking of high-speed trajectories," *IEEE Robotics and Automation Letters*, vol. 3, no. 2, pp. 620–626, 2018.

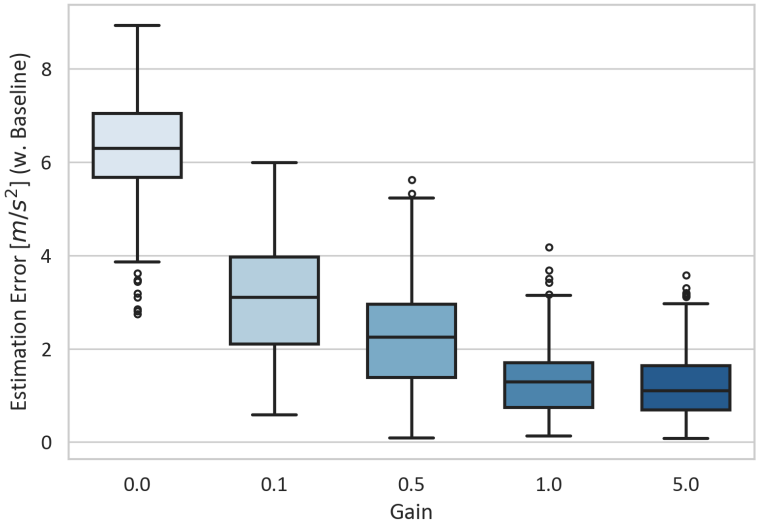

Fig. A6. Ablation Study on different adaptation gains.